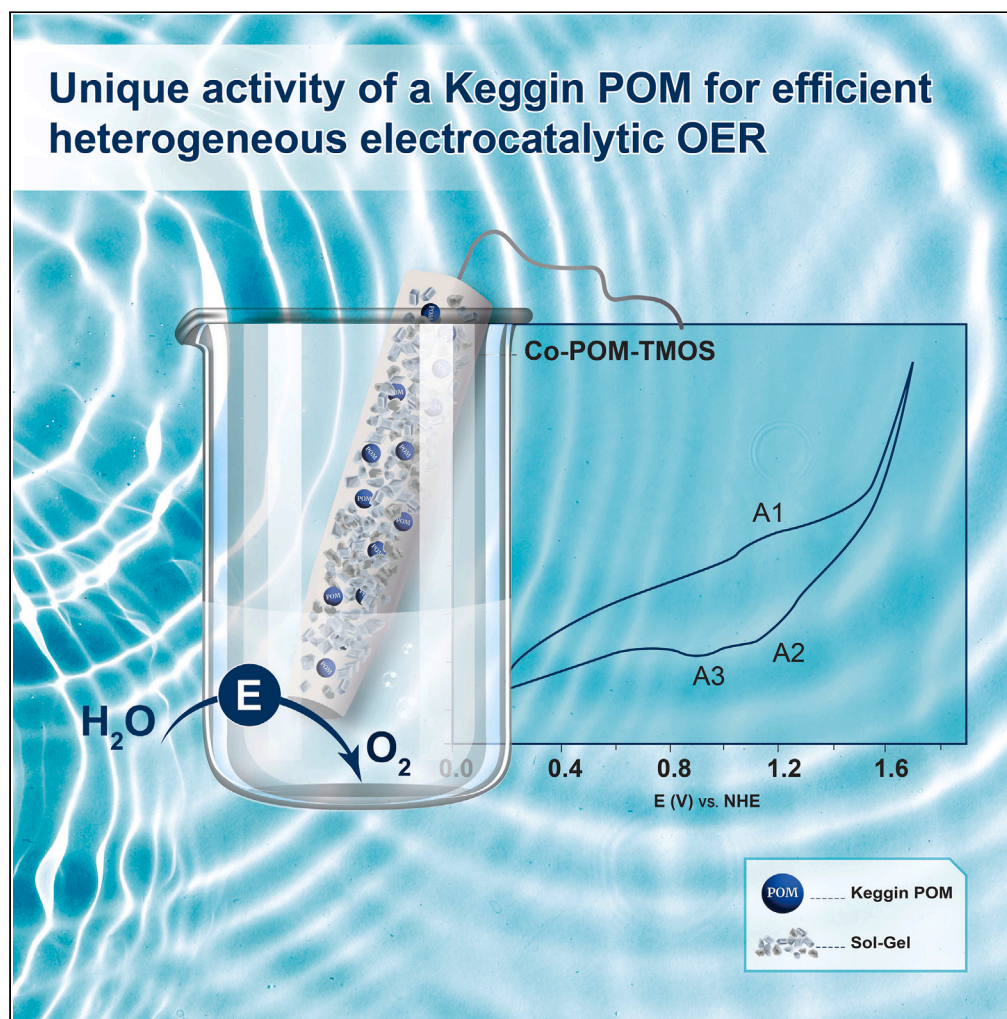**Article**

Unique activity of a Keggin POM for efficient heterogeneous electrocatalytic OER

Chandani Singh,
Dan Meyerstein,
Zorik Shamish,
Dror Shamir, Ariela
Burg

drorshamir@gmail.com (D.S.)
arielab@sce.ac.il (A.B.)

Highlights
Keggin POM was
entrapped for the first time
in a sol-gel matrix

The Co-POM-TMOS
electrode could be reused
for OER for more than 90
days

The sol-gel matrix
stabilizes Co-POM under
electrochemical conditions
at pH 2

Article

Unique activity of a Keggin POM for efficient heterogeneous electrocatalytic OER

Chandani Singh,[1,2] Dan Meyerstein,[2,3] Zorik Shamish,[4] Dror Shamir,[4,*] and Ariela Burg[1,5,*]
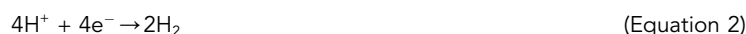
SUMMARY

Polyoxometalates (POMs) have been well studied and explored in electro/photochemical water oxidation catalysis for over a decade. The high solubility of POMs in water has limited its use in homogeneous conditions. Over the last decade, different approaches have been used for the heterogenization of POMs to exploit their catalytic properties. This study focused on a Keggin POM, $K_6[CoW_{12}O_{40}]$, which was entrapped in a sol-gel matrix for heterogeneous electrochemical water oxidation. Its entrapment in the sol-gel matrix enables it to catalyze the oxygen evolution reaction at acidic pH, pH 2.0. Heterogenization of POMs using the sol-gel method aids in POM's recyclability and structural stability under electrochemical conditions. The prepared sol-gel electrode is robust and stable. It achieved electrochemical water oxidation at a current density of 2 mA/cm^2 at a low overpotential of 300 mV with a high turnover frequency (TOF) of 1.76 [mol O_2 (mol Co)$^{-1}$s^{-1}]. A plausible mechanism of the electrocatalytic process is presented.

INTRODUCTION

The energy crisis and increased environmental issues in the current social development scenario have motivated everyone to find alternative energy sources and sustainable ways to store this energy.[1–3] Using fossil fuels, which most countries' energy systems are based on,[4] causes climate change and global warming.[5,6] This has highlighted the need for new sustainable and renewable energy sources that are cost-competitive compared to crude oil and coal.[7]

As a carbon-free energy source, hydrogen is a promising energy carrier. Therefore, a sustainable and greener approach can be used for energy development and storage.[8–12] Electrochemically splitting water is one method that obtains the hydrogen required for hydrogen energy. The water splitting process (WSP), comprises two half-reactions: oxygen evolution reaction (OER), and hydrogen evolution reaction (HER), reactions 1 and 2 at acidic solutions and 3 and 4 at basic solutions.

$$2H_2O \rightarrow O_2 + 4H^+ + 4e^- \qquad \text{(Equation 1)}$$

$$4H^+ + 4e^- \rightarrow 2H_2 \qquad \text{(Equation 2)}$$

$$4OH^- \rightarrow O_2 + 2H_2O + 4e^- \qquad \text{(Equation 3)}$$

$$4H_2O + 4e^- \rightarrow 2H_2 + 4OH^- \qquad \text{(Equation 4)}$$

Due to sluggish kinetics and high thermodynamics barrier, OER is considered the bottleneck process for water splitting; hence the need to develop catalysts for OER.[13–17] The unfavorable kinetics of this reaction under neutral or alkaline electrolytes necessitates highly efficient electrocatalysts in acidic conditions. Acidic conditions reduce the overpotential and accelerate the reaction rate.[18–20] Therefore, HER is favored in acidic conditions due to the high concentration of protons and proton exchange membranes that can support high current densities (greater than 1 A/cm^2), minimizing the crossover and resistance losses.[21–25] Hence, by designing a catalyst for OER at low pH, the overall energy requirement for water splitting could be substantially reduced.[26,27]

Electrochemical OER catalysis under acidic pH poses a challenge as many well-known catalysts of electrochemical OER suffer from structural instability at low pH levels (acidic condition).[28,29] Well-known catalysts for acidic OER are precious metal oxides such as IrO_2 and RuO_2.[30–32] In the last few years, many catalysts comprising earth-abundant metal oxides were reported for electrochemical acidic OER, but molecular catalyst are still scarce.[30,31] Most molecular catalyst comprise organic ligands that protonate at low pH, disrupting the structural stability of such compounds.[33] Designing a molecular catalyst for acidic OER could help understand the kinetics at the molecular level and, in

[1]Department of Chemical Engineering, Sami Shamoon College of Engineering, Beer-Sheva, Israel
[2]Chemistry Department, Ben-Gurion University of the Negev, Beer-Sheva, Israel
[3]Chemical Sciences Department, Ariel University, Ariel, Israel
[4]Analytical Chemistry Department, Nuclear Research Center Negev, Beer-Sheva, Israel
[5]Lead contact
*Correspondence: drorshamir@gmail.com (D.S.), arielab@sce.ac.il (A.B.)
https://doi.org/10.1016/j.isci.2024.109551

turn, could help devise a better OER catalyst. In this regard, polyoxometalates (POMs), a molecular oxide containing only inorganic units with excellent structural stabilities at low pH values, can be an alternative approach. There are few reports with different POMs as electrochemical OER catalysts at low pH.[34–40]

POMs belong to a particular class of metal oxides that self-assemble under different reaction conditions to acquire interesting structures.[41–45] POMs generally consist of transition metals that are connected by an oxo-bridge. The reaction conditions during the synthesis of these oxyanions play a critical role in assembling POMs. Keggin POMs, belong to a class of hetero-polyanions, have the general formula of $[XM_{12}O_{40}]^{n-}$ where X is a heteroatom (such as $Si^{IV}/P^{III}/Co^{II}/Fe^{II}$) and M is an addenda atom (e.g., M = W^{6+}/Mo^{6+}).[36,46,47] The central atom forms a tetrahedron, which corresponds to "XO_4". This "XO_4" unit shares the vertices with the four "M_3O_{13}" (triad). The oxygen in the "XO_4" unit is shared by the MO_6 octahedral, which forms the triad. The activation of the central heteroatom (X), surrounded by the addenda (M) oxides, for catalyzing the electrochemical water oxidation process is challenging. The highly accepted and predominantly proposed mechanism for water oxidation is the water nucleophilic attack (WNA) to the high-valent metal-oxo species or metal-oxyl radicals, where O–O bonds are formed. In the case of Keggin POM, such a WNA mechanism is not probable due to the unavailability of a site for a water molecule to attack the heteroatom (X).[36] Hence, the majority of POM-based water oxidation catalysts (WOC) are Keggin-derived POMs, such as lacunary Keggin POM or sandwiched POMs.[48–50] In 2018, Mukhopadhyay et al. reported a Keggin POM, $K_6[CoW_{12}O_{40}]$ (Co-POM), as a WOC which could only be achieved by encapsulating it into ZIF-8 cavity.[36] The change in the microenvironment around the POM due to the encapsulation made it stable toward electrocatalytic OER at neutral pH.[36] Following this study, the Co-POM was again studied by hydrogenizing using ionic liquids and fabricating it onto a graphene surface, exhibiting great catalytic behavior.[51]

The first-ever report for water oxidation by POM was made by Sortel et al. 2008.[52] They reported a di-γ-decatungstosilicate embedding a tetra-ruthenium(IV)-oxo core as a water oxidation catalyst where a Ru^{IV} center was the active site for the catalysis.[52] In 2011, Yin et al., reported a Co-based sandwiched POM, $[Co_4(H_2O)_2(B-\alpha-PW_9O_{34})_2]^{10-}$ for OER catalysis.[53] This work revolutionized the POM chemistry and helped designing and understanding POM-based OER catalysts.[35,54,55] Due to POM's high solubility in an aqueous medium, most POM-based electrocatalytic OER studies are done in a homogeneous medium.[35,56,57] This limits their catalytic study to homogeneous aqueous conditions, which reduces the recyclability of the catalyst as well as the feasibility of the process. There are many approaches studied till now in an effort to heterogenize POMs, increasing their reusability.[36,58–60] One such technique is to entrap the POM anion within a matrix such as sol-gel. The sol-gel matrix is common for the entrapment of various active species such as organic and inorganic compounds, nanoparticles of metals and metal oxides, enzymes, and many more active species.[27,61–66] Preparing SiO_2-based matrices using the sol-gel method has gained attention due to the simplicity and versatility of the process. Recent results indicate that the pH affects the k_{cat} of the electrochemical process, and the sol-gel precursors type affect the hydrophobicity of the matrix and influence the electro-catalytic process.[27] Those features of the sol-gel matrix could improve the OER process; therefore, in the present work, we used the sol-gel process to entrap POM inside a sol-gel matrix and prepare a stable, robust, heterogenized POM for electrocatalytic OER at acidic pH. The sol-gel matrix provides stability and heterogeneity to the POM, allowing the recyclability of the electrode for prolonged use and making it a sustainable and feasible approach.[67,68]

In this work, we have used a Keggin POM, $K_6[CoW_{12}O_{40}]$, entrapped in a sol-gel matrix prepared from tetramethyl orthosilicates (TMOS) to prepare the working electrode for OER. The prepared electrode is highly robust and stable in the electrochemical OER process. This work is the first of its kind where a Keggin POM, $K_6[CoW_{12}O_{40}]$, which is entrapped in a sol-gel matrix, and is used as an electrocatalyst for the acidic OER. This study opens up new pathways for designing molecular catalysts for efficient electro-catalysis processes.

RESULTS AND DISCUSSION

Synthesis, fabrication, and morphology

The sol-gel electrodes, Co-POM-TMOS (working sol-gel electrode with $K_6[CoW_{12}O_{40}]$), and TMOS (working sol-gel electrode without $K_6[CoW_{12}O_{40}]$) electrodes (Table S3) were prepared following the protocol aforementioned and characterized using experimental techniques such as powder X-ray diffraction (PXRD) (Figure 1A), X-ray photoelectron spectroscopy (XPS) (Figures 1B and S4), fourier-transform infrared spectroscopy (FTIR) (Figure S3), Raman spectroscopy (Figure S5), and energy-dispersive X-ray spectra (EDX) (Table S1).

As a control, a set of Co-POM-TMOS electrodes (Table S3) was prepared for characterization without graphite so that the strong features of carbon/graphite could be avoided from the experimentally obtained physical characterizations. It was used for PXRD. The PXRD obtained was compared with the simulated PXRD pattern of Co-POM (Figure 1A). The PXRD confirms the entrapment of Co-POM inside the TMOS sol-gel matrix. Only the main peaks are seen in the PXRD spectrum, this could be because of the binding of the Co-POM to the sol-gel matrix.[68] (Figure 1A). The matched PXRD pattern is also an indirect proof of the Co-POM to be present in the hybrid heterogeneous electrode prepared from TMOS sol-gel matrix.

The comparative study of FTIR analysis of Co-POM, Co-POM-TMOS, TMOS sol-gel electrodes, and Co-POM confirms the successful entrapment of Co-POM inside the sol-gel matrix (Figure S3).

The characteristic IR stretching of Co-POM arising from W-O-W and W=O could be spotted for the Co-POM-TMOS sol-gel electrode with a negligible shift in any of this IR stretching. The IR stretching for Co-POM-TMOS; 942, 882, 766, 452 cm^{-1}. Furthermore, XPS was performed for both the Co-POM-TMOS electrodes and Co-POM (Figures 1B and S4 for tungsten and oxygen, respectively. The cobalt couldn't be detected by XPS[69]). The X-ray photoelectron spectra of W_{4f} of Co-POM-TMOS were similar to that of Co-POM (the spectrum of the latter is similar to the published spectrum[36]) with no significant shift and directed toward +6 oxidation state of W (Figure 1B). The small shift of the Co-POM-TMOS, compared to Co-POM, could be due to the covalent binding of Co-POM to the matrix, which is supported by published results.[68]
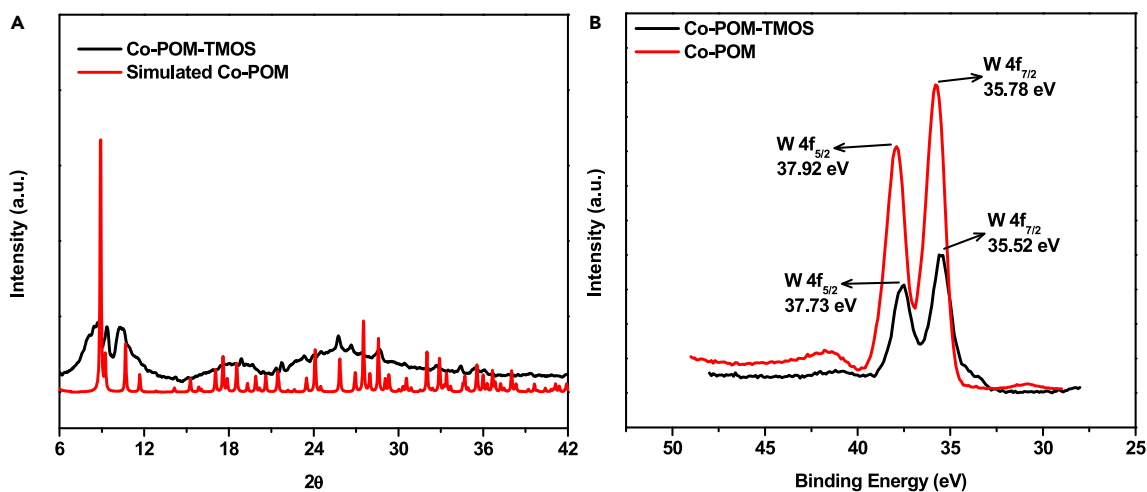
Figure 1. Physical characterization of Co-POM-TMOS
(A) Powder-XRD of Co-POM-TMOS compared with simulated PXRD pattern of Co-POM.
(B) XPS of Co-POM-TMOS sol-gel electrode and Co-POM.

Thus, with the help of various physical characterizations, we could successfully prove the entrapment of Co-POM in the sol-gel matrix in the case of Co-POM-TMOS sol-gel electrode and also understood the modifications of the electronic properties of both the constituents of the guest entrapped sol-gel matrix. Heterogenization followed by modification of the electronic properties of the Co-POM can be advantageous for electrochemical applications. Thus, we were interested in studying the Co-POM-TMOS sol-gel electrode's electrochemical behavior and comparing it with its constituents i.e., the TMOS sol-gel and the Co-POM.

Electrochemical characterization

The Co-POM-TMOS sol-gel electrodes were studied as working electrodes by cyclic voltammetry (Figure 2). The electrodes showed three redox waves labeled A1, A2, and A3 at 1.15–1.16 V, 1.11–1.12 V, and 0.91–0.92 V, respectively (Figure 2A).

A reduction peak A2 at 1.11–1.12 V is observed for both TMOS sol-gel electrode and Co-POM-TMOS sol-gel electrode. The redox peaks A1 and A3 represent the Co^{II} to Co^{III} oxidation reaction and Co^{III} to Co^{II} reduction reaction, respectively.[70] The redox peak A1 seen in the cyclic voltammogram (CV) of the Co-POM-TMOS sol-gel electrode is followed by a current arising due to water oxidation with an onset
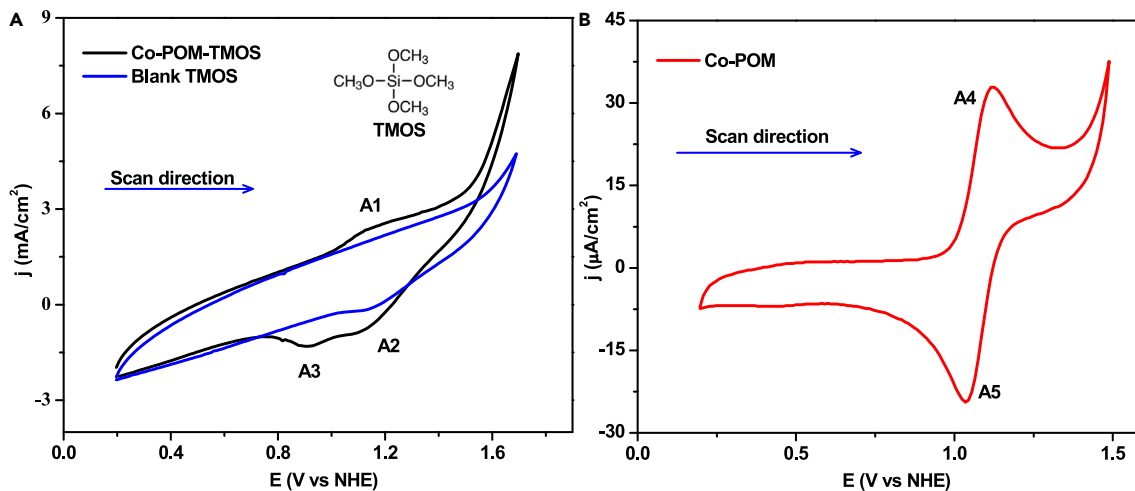

Figure 2. Electrochemical characterization of Co-POM-TMOS
CVs in solutions containing 0.20 M $NaClO_4$ at pH 2, at a scan rate of 20 mV/s. (A) Co-POM-TMOS sol-gel electrode and TMOS sol-gel electrode as working electrodes.
(B) Glassy carbon electrode as a working electrode. The solution contains 1.0 mmol Co-POM.
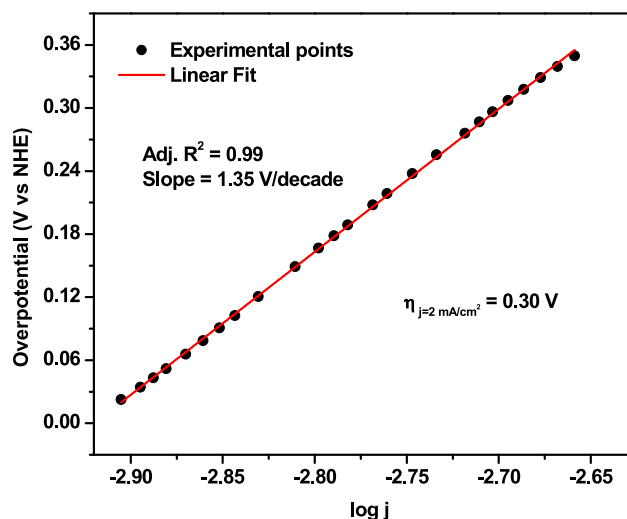
Figure 3. Tafel plot of oCo-POM-TMOS
iR-corrected, Recorded in 0.2 M NaClO$_4$, pH 2.

potential of 1.52 V. No such onset current is seen for TMOS sol-gel electrode referring to the catalysis by Co-POM entrapment in the matrix of TMOS based sol-gel. The redox potentials in the homogeneous system are similar to the redox potentials in the heterogeneous system (an anodic peak A4 at 1.1 V and cathodic peak A5 at 1.0 V) as seen in the homogeneous system (Figure 2B).[70] CVs for Co-POM-TMOS sol-gel electrodes were recorded by varying the scan rate (Figure S6). The anodic peak current and the cathodic current concerning the root of the scan rate follow a linear relationship (Figures S7 and S8),[60] which could be inferred to diffusion-controlled redox reaction as well as a catalytic process for Co-POM-TMOS sol-gel electrodes.

Comparing the cyclic voltametric results, it can be concluded that the electrochemical OER of the Co-POM-TMOS sol-gel-electrode is due to the Co-POM entrapment. Co-POM acts as the active catalytic center for the electrocatalytic OER. The entrapment of Co-POM in the sol-gel electrode permits the Co-POM to act as a catalyst in OER at pH as low as 2.0.

To further understand the electrochemical OER performed by Co-POM-TMOS sol-gel electrode, the kinetic parameters of the electrochemical OER were determined and analyzed.

The turnover frequency (TOF) was determined by calculating the surface coverage of electrochemically active "Co" species as described in STAR Methods Section, by constructing the plot of anodic peak current vs. scan rate (Figure S9). The TOF obtained for Co-POM-TMOS sol-gel electrode is 1.76 [mol O$_2$ (mol Co)$^{-1}$s^{-1}]. The overpotential of OER was calculated by constructing a Tafel plot (Figure 3). Tafel plot was derived from the catalytically active region of a linear scan voltammogram (LSV) of Co-POM-TMOS sol-gel electrode recorded at an extremely low scan rate (1 mV/s) (Figure S10).

The overpotential requirement for the Co-POM-TMOS sol-gel electrode was found to be 300 mV (at the current density of 2 mA/cm^2). The observed overpotential requirement is lower for Co-POM-TMOS sol-gel electrode than most other Keggin-based heterogeneous systems reported (Table 1).

Moreover, high observed TOF combined with the requirement of low overpotential for electrochemical OER at low pH makes Co-POM-TMOS sol-gel electrode a promising candidate for electrocatalytic OER studies. Similar electrocatalytically active systems can be designed using POMs, which will be entrapped in sol-gel matrix in the future. The CV features show a resistive behavior of the Co-POM-TMOS sol-gel electrode arising from the TMOS sol-gel compared with the homogeneous Co-POM.

The electrochemical surface area (ECSA) for the Co-POM-TMOS and TMOS sol-gel electrodes was calculated using the CVs recorded in the non-faradic region at various scan rates (Figures 4, S11, and S12).[21,74]

The double-layer capacitance (C$_{dl}$) of Co-POM-TMOS and TMOS sol-gel electrodes is 16.57 μF/cm^2 and 8.55 μF/cm^2, respectively (Figure 4). Generally, the ECSA is directly proportional to the determined C$_{dl}$ values according to Equations 5 and 6:

$$ECSA = \frac{Cdl}{Cs}$$

(Equation 5)

$$\frac{ECSA\,1}{ECSA\,2} = \frac{Cdl\,1}{Cdl\,2}$$

(Equation 6)

As observed from Figure 4, the C$_{dl}$ of Co-POM-TMOS is two times the C$_{dl}$ of TMOS sol-gel electrode. The same should be the trend of the ECSA of the Co-POM-TMOS and TMOS sol-gel electrodes. Thus, the Co-POM entrapment inside the sol-gel matrix increases the ECSA. The increase in the ECSA can be considered an essential factor behind the increased electrochemical OER performance of the Co-POM-TMOS electrode. The high ECSA of the Co-POM-TMOS electrode signifies that the *in-situ* entrapment of the Co-POM in the hydrophilic and highly

Table 1. Comparison of overpotential of different POM related heterogeneous OER catalysts

Compound	Op @ 1mA/cm^2	Reference
[Ni(2,2-bpy)$_3$]$_5$[PW$_{11}$NiO$_{39}$(H$_2$O)]$_2$ · 1.08H$_2$O	591 mV	Wang et al., 2016[71]
Ni(2,2-bpy)$_3$]$_{1.5}$[Ni(2,2-bpy)$_2$(H$_2$O)BW$_{12}$O$_{40}$]	632 mV	Wang et al., 2016[71]
{[Ni(2,2bpy)$_3$]$_{1.5}$[Ni(2,2bpy)$_2$(H$_2$O)PW$_{12}$O$_{40}$] }$^{2-}$	616 mV	Wang et al., 2016[71]
{[Ni^{II}(2,2′-bpy)$_2$(H$_2$O)][Ni^{II}(2,2′-bpy)$_3$]$_{1.5}$} [H(Co^{II}W$_{12}$O$_{40}$)]·2H$_2$O}	457 mV	Singh et al., 2018[60]
([NiL](PF$_6$)$_2$ (L = bis(2-pyridyl-methylimidazolylidene) methane)	800 mV @ 0.65 mA/cm^2	Shahadat et al., 2019[72]
5,15-diphenylporphinatonickel(II)	400 mV @ 0.7 mA/cm^2	Krishna et al., 2018[73]
[H$_6$CoW$_{12}$O$_{40}$] @ ZIF-8	784.19 mV	Mukhopadhyay et al., 2018[36]
Co-POM-TMOS	300 mV @ 2 mA/cm^2	Present Work

porous matrix of TMOS sol-gel matrix can be considered as an efficient strategy for developing POM-based heterogeneous electrodes. In this regard, choosing the appropriate sol-gel matrix can be crucial. The role of porosity and hydrophilicity of TMOS sol-gel matrix cannot be neglected behind the observed ECSA of the hybrid electrode.

Furthermore, an overall decrease in the resistance was observed as a result of the entrapment of the Co-POM in the TMOS sol-gel, from the Nyquist plot obtained by electrochemical impedance spectroscopy (EIS) measurement shown in Figure 5.

We fitted the Nyquist plot with the equivalent circuit "R1+C1/(R2+Q2/R3)+C4/R4" depicted in Figure S13. As expected, with the introduction of POM molecule in the sol-gel cavity, a drop in R$_s$ is observed. The parameters of each component are provided in Table S4 in the Supporting Information. A considerable decrease in the bulk resistance (Rs) for the Co-POM-TMOS sol-gel electrode compared to the TMOS sol-gel electrode can be observed from the EIS measurements. Such lowering of R$_S$ is advantageous for electrocatalytic applications. Entrapment of Co-POM inside the hydrophilic porous matrix of TMOS with the scope of electrostatic interactions between the POM anions i.e., [CoW$_{12}$O$_{40}$]$^{6-}$, and TMOS causes this lowering of the overall resistance of the hybrid electrode because POMs are well-known for being efficient charge transfer agents. Besides helping the charge transport process, the Co-POM, in case of Co-POM-TMOS is also the catalytically active center for the electrocatalytic OER. This implies that the ease of electron transport in Co-POM-TMOS may have helped the observed catalytic process. The efficient charge transfer may have contributed along with the hydrophilicity and porosity of the sol-gel matrix behind the high ECSA observed for Co-POM-TMOS.

As indicated by the high slope (1.35 V/decade) of the Tafel plot (Figure 3) a proton-coupled sluggish multi-electron transfer process can occur as the rate-determining step. Furthermore, a detailed understanding of the structural properties of the nano particular metal oxide i.e., the Co-POM, which is the molecular electrocatalyst in the case of Co-POM-TMOS sol-gel electrode, can help to understand the complex electrochemical process happening during the catalytic OER. The data obtained are not sufficient to prove a detailed mechanism of the electro-catalytic process reported; however, some ideas concerning the plausible mechanism are justified; considering the structure of the Keggin POM, it is unlikely that the central Co$^{V/IV}$ can bind to the water molecule, which in this case, is the substrate. The following mechanism seems probable:
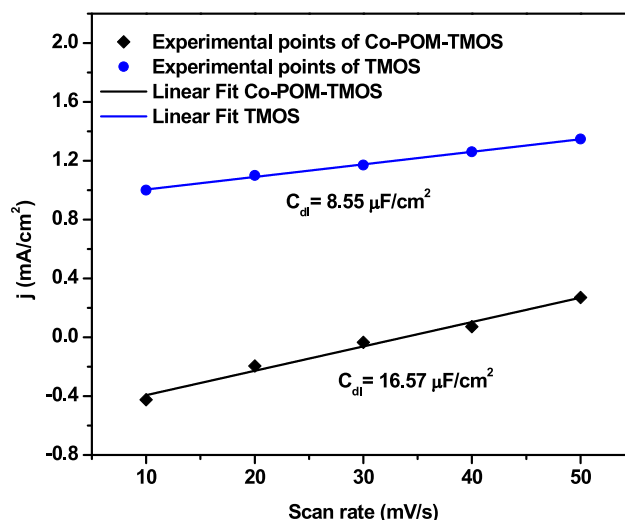

Figure 4. Electrochemical surface area (ECSA) for the Co-POM-TMOS and TMOS sol-gel electrodes
Linear fits for the anodic current @ 0.41 V (vs. NHE) for CO-POM-TMOS and TMOS sol-gel electrodes.
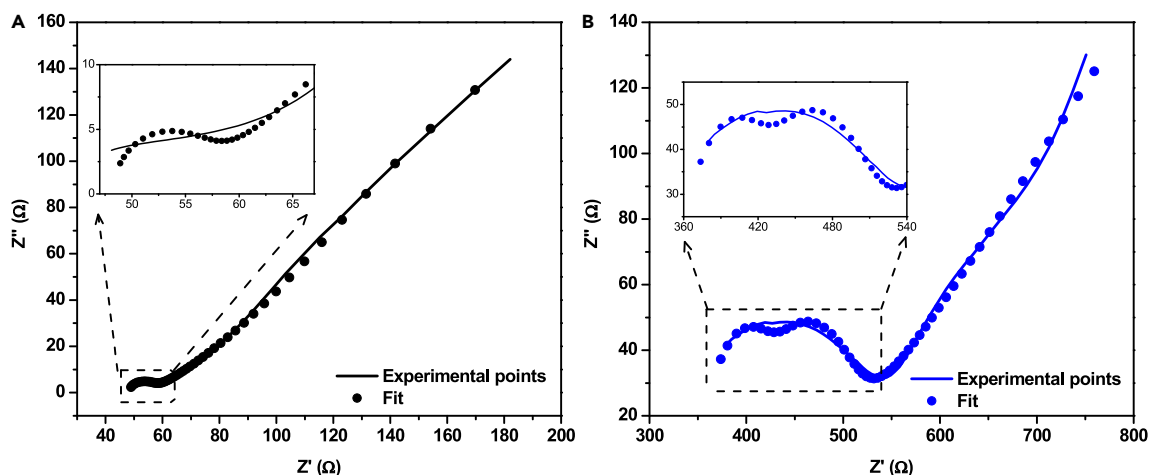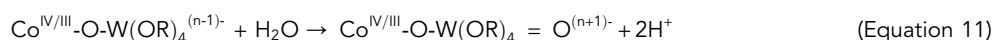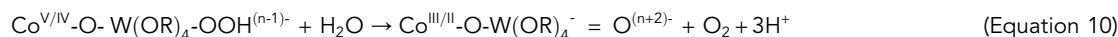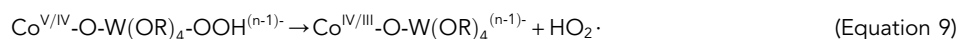
Figure 5. EIS measurements of Co-POM-TMOS and TMOS

Nyquist plot of (A) Co-POM-TMOS and (B) TMOS sol-gel electrodes, recorded in 0.2 M NaClO$_4$ and pH 2.

$$Co^{V/IV}\text{-O-W(OR)}_4 = O^{n-} + H_2O \rightarrow Co^{III/II}\text{-O-W(OR)}_4\text{-OOH}^{(n+1)-}H^+ \qquad \text{(Equation 7)}$$

$$Co^{III/II}\text{-O-W(OR)}_4\text{-OOH}^{(n+1)-}\text{-}2e^- \rightarrow Co^{V/IV}\text{-O-W(OR)}_4\text{-OOH}^{(n-1)-} \qquad \text{(Equation 8)}$$

$$Co^{V/IV}\text{-O-W(OR)}_4\text{-OOH}^{(n-1)-} \rightarrow Co^{IV/III}\text{-O-W(OR)}_4^{(n-1)-} + HO_2\cdot \qquad \text{(Equation 9)}$$

$$Co^{V/IV}\text{-O- W(OR)}_4\text{-OOH}^{(n-1)-} + H_2O \rightarrow Co^{III/II}\text{-O-W(OR)}_4^- = O^{(n+2)-} + O_2 + 3H^+ \qquad \text{(Equation 10)}$$

$$Co^{IV/III}\text{-O-W(OR)}_4^{(n-1)-} + H_2O \rightarrow Co^{IV/III}\text{-O-W(OR)}_4 = O^{(n+1)-} + 2H^+ \qquad \text{(Equation 11)}$$

Reaction (7) is analogous to the commonly accepted mechanism of water oxidation by high-valent metal oxides.[75] Reaction (8) is an anodic process. Reactions (9)–(11) are reasonable steps. Since POM is well-known to be an efficient charge transfer agent, the electron transfer to the central Co$^{V/IV}$ is reasonable (it is known from the literature that the POM without cobalt, for example [PW$_{12}$O$_{40}$]$^{3-}$ and [SiW$_{12}$O$_{40}$]$^{4-}$ are used for HER[76]). The electrochemical stability of the prepared sol-gel electrodes was confirmed by constant potential electrolysis (CPE) at 1.6 V, and LSV measurements are presented in Figure 6.

From constant potential electrolysis (CPE) measurement in Figure 6A, the Co-POM-TMOS electrode was found to be stable for more than 30 min, and this measurement was taken after reusing the electrode repetitively for more than two months. As shown in Figure 6B, The LSV recorded after the electrochemical studies are in good comparison with LSV recorded with the new electrode. The same electrodes were dried completely and were used for spectroscopic analysis and relevant physical characterizations to understand the electrochemical study and reusability of the Co-POM-TMOS hybrid sol-gel electrode.

The structural stability of the electrodes was studied by spectral analysis before and after electrochemical studies (Figure 7).

The Raman Spectral analysis and FTIR spectra of Co-POM-TMOS sol-gel electrode before and after the electrochemical study for Co-POM-TMOS are similar, with no significant changes. This result indicates that the sol-gel electrodes are stable, and the matrix saves the Co-POM structure even after the electrocatalytic OER.

SEM images were recorded for the electrodes (Figure 8) before and after the electrochemical study to check for any change in their morphology, but no such changes were observed.

Energy-dispersive spectra (EDS) analysis was done for all the electrodes to check the elemental composition. The chemical composition of the Co-POM-TMOS sol-gel electrodes before and after the electrochemical studies was similar. This also points toward the stability of the catalyst, Table S1.

The inductively coupled plasma (ICP) analysis of the electrolyte after the CPE analysis was done to check for any leaching of the metal ions into the electrolyte. The results are presented in Table S2. The results prove that some slow leaching of Co-POM into the solution occurs, the structural integrity of Co-POM remains intact. The leaching could be associated to the hydrophilic nature of TMOS, due to which water is entering inside the electrode-holder and since, the interaction between POM and matrix is only electrostatic interaction, once, in contact with water, the high solubility of Co-POM in water leads to this slow leaching.

The sol-gel electrodes were prepared with maintaining the pH of the solution phase at approximately 2 or slightly below 2. The point of zero charge (PZC) of Si-OH-containing TMOS lies between pH 1.5–4.5.[77] For the pH of the precursor solution of the sol-gel electrode 2 or below, the accumulation of positive charge on the siliceous species could be observed.[78] TMOS, being hydrophilic in nature, once these
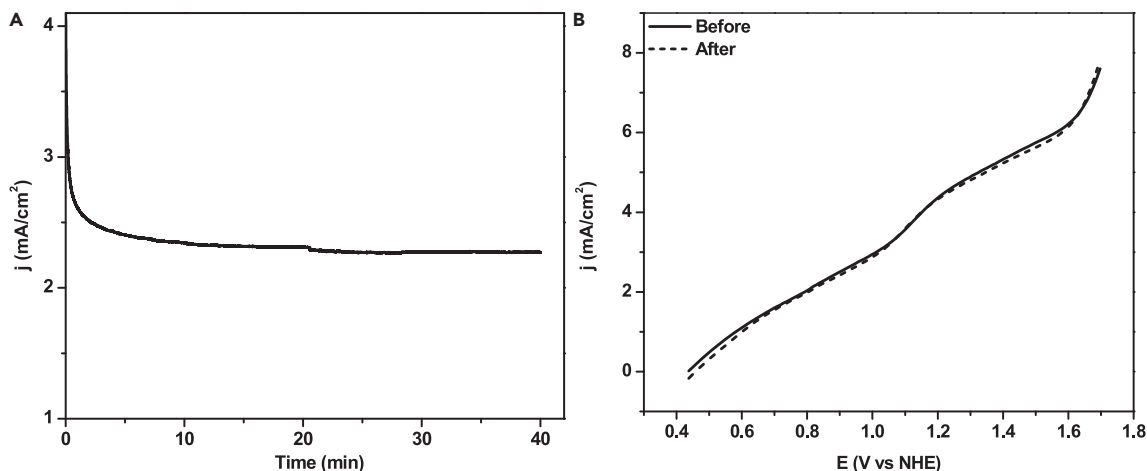
Figure 6. Electrochemical stability of Co-POM-TMOS electrode

(A) Constant Potential Electrolysis (CPE) recorded at 1.6 V for Co-POM-TMOS sol-gel electrode.

(B) Comparison of LSVs of Co-POM-TMOS before and after continuous reusing for electrochemical study for 30 days, scan rate: 50 mV/s, 0.2 M NaClO₄, pH 2.

electrodes are dipped in aqueous solutions, a capillary action could be seen by which water enters the matrix. Interestingly, Co-POM in aqueous solution possesses an inherent high negative charge as it loses the protons in the process of solvation. Thus, the $[CoW_{12}O_{40}]^{6-}$ anion, with the high negative charge should be getting trapped in the sol-gel matrix in the process of the electrode formation.

The experimental condition of the preparation of the electrodes (a low pH of pH 2), suggests that the resulting electrodes should have high negatively charged $[CoW_{12}O_{40}]^{6-}$ anion trapped inside the sol-gel matrix bearing excess of positive charge, leading to highly probable electrostatic interaction between the POM anion and the matrix. As a result of these electrostatic interactions, POM anions are stabilized in the sol-gel matrix and promote the catalytic OER process under acidic conditions. The probability that the active species in the OER is free cobalt, which is released from the POM, is low, which is also according to the literature.[35,79]

Conclusions

In this work, we have designed and studied a Keggin POM sol-gel electrode by entrapping $K_6[CoW_{12}O_{40}]$, for electrocatalytic OER for the first time. The Co-POM-TMOS sol-gel electrode is highly robust and can be reused for electrocatalytic OER for more than 90 days with a low overpotential of 300 mV and high TOF of 1.76 $[mol\ O_2\ (mol\ Co)^{-1}s^{-1}]$. Heterogenization of Co-POM, using a hydrophilic sol-gel precursor, results in electrostatic interaction between the POM and the matrix. The composite, thus prepared, allows facile hydrogen bonding of water molecules onto the surface of Co-POM. Our results indicate that the Co-POM-TMOS sol-gel electrodes stabilize the structural integrity of
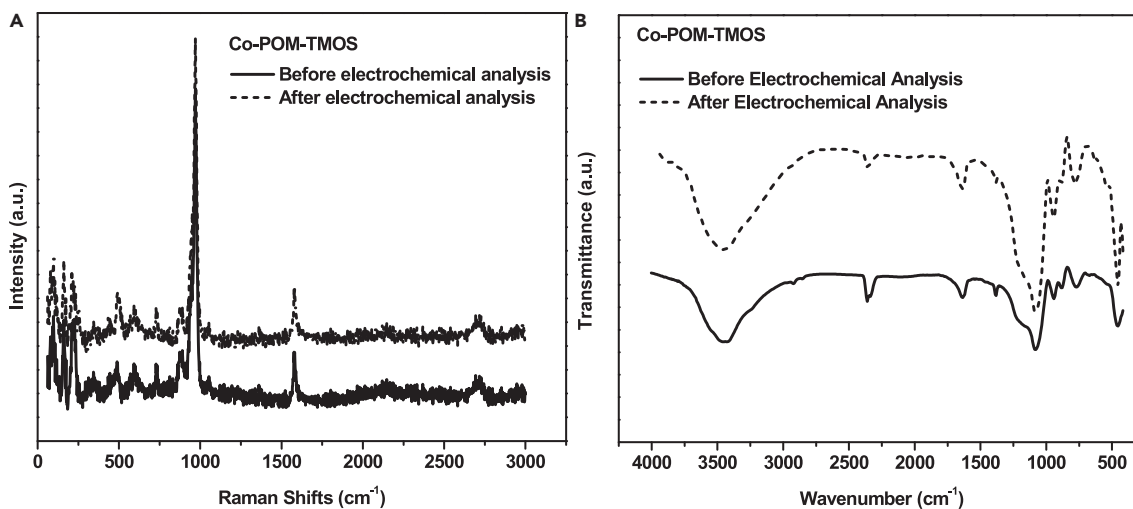

Figure 7. Structural stability of Co-POM-TMOS electrode

Spectral analysis of Co-POM-TMOS before and after the electrochemical study using (A) Raman analysis, (B) FT-IR analysis.
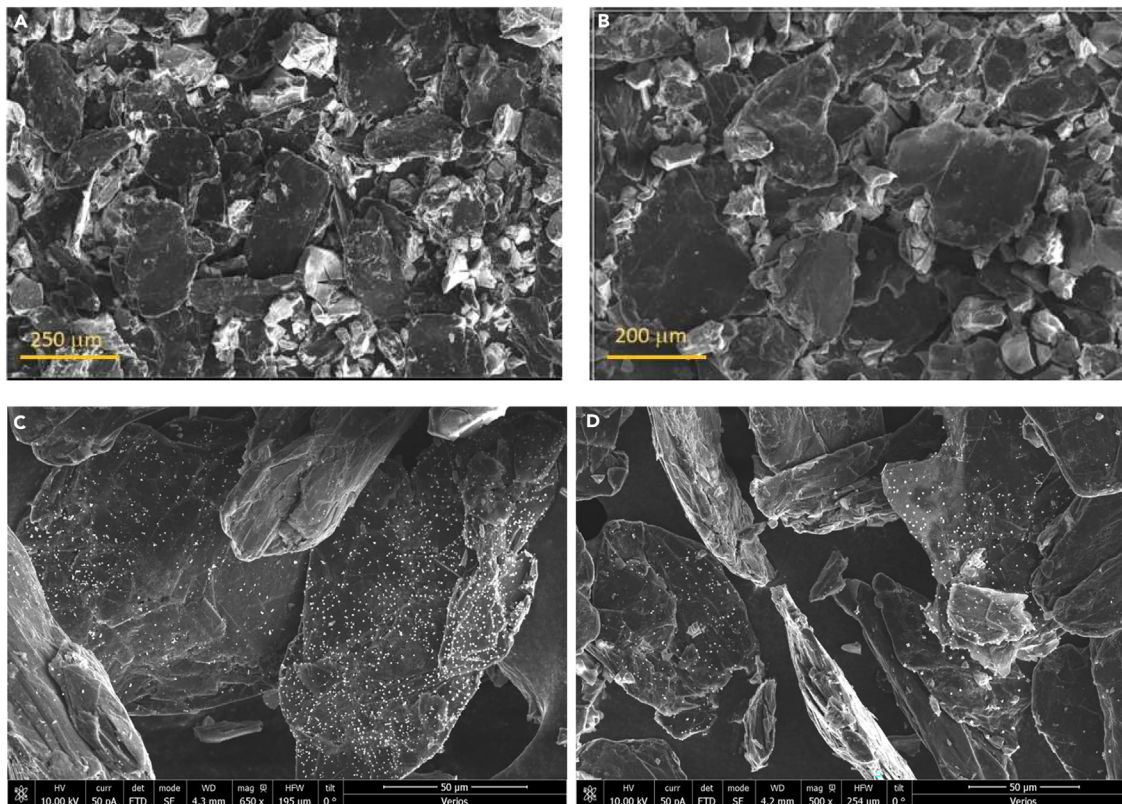
Figure 8. Morphological stability of Co-POM-TMOS electrode
SEM images of the Co-POM-TMOS sol-gel electrodes were recorded (A and C) before and (B and D) after the electrochemical analysis.

Co-POM under electrochemical conditions of OER catalysis at pH 2. According to the results a plausible mechanism for the electrocatalytic OER process is outlined.

Limitations of the study

The research is mainly based on electrochemical results with a unique sol-gel electrode for heterogeneous OER, which are supported through several electrochemical techniques, such as EIS and CV. The results and mechanism only represent the specific POM that were synthesized and studied in this research.

STAR★METHODS

Detailed methods are provided in the online version of this paper and include the following:

- KEY RESOURCES TABLE
- RESOURCE AVAILABILITY
  - Lead contact
  - Materials availability
  - Data and code availability
- METHOD DETAILS
  - Materials
  - Co-POM synthesis
  - Working electrode preparation
  - Blank electrode preparation
  - Characterization methods
  - Electrochemical studies
- QUANTIFICATION AND STATISTICAL ANALYSIS
  - Calculation of surface coverage and number of active cobalt atoms
  - Calculation of turnover frequencey (TOF) for O_2 evolution from Tafel plot

REFERENCES

1. Mikhaylov, A. (2022). Sustainable Development and Renewable Energy: A New View to a Global Problem. Energies 15, 1397.

2. Apollon, W., Rusyn, I., González-Gamboa, N., Kuleshova, T., Luna-Maldonado, A.I., Vidales-Contreras, J.A., and Kamaraj, S.-K. (2022). Improvement of zero waste sustainable recovery using microbial energy generation systems: A comprehensive review. Sci. Total Environ. 817, 153055. https://doi.org/10.1016/j.scitotenv.2022.153055.

3. Khoshnevisan, B., He, L., Xu, M., Valverde-Pérez, B., Sillman, J., Mitraka, G.-C., Kougias, P.G., Zhang, Y., Yan, S., Ji, L., et al. (2022). From renewable energy to sustainable protein sources: Advancement, challenges, and future roadmaps. Renew. Sustain. Energy Rev. 157, 112041. https://doi.org/10.1016/j.rser.2021.112041.

4. Caetano, N.S., Mata, T.M., Martins, A.A., and Felgueiras, M.C. (2017). New Trends in Energy Production and Utilization. Energy Proc. 107, 7–14. https://doi.org/10.1016/j.egypro.2016.12.122.

5. Gizer, S.G., Polat, O., Ram, M.K., and Sahiner, N. (2022). Recent developments in CO2 capture, utilization, related materials, and challenges. Int. J. Energy Res. 46, 16241–16263. https://doi.org/10.1002/er.8347.

6. Ullas Krishnan, J.N., and Jakka, S.C.B. (2022). Carbon dioxide: No longer a global menace: A future source for chemicals. Mater. Today: Proc. 58, 812–822. https://doi.org/10.1016/j.matpr.2021.09.271.

7. Al-Shetwi, A.Q. (2022). Sustainable development of renewable energy integrated power sector: Trends, environmental impacts, and recent challenges. Sci. Total Environ. 822, 153645. https://doi.org/10.1016/j.scitotenv.2022.153645.

8. Kumar, A., Daw, P., and Milstein, D. (2022). Homogeneous Catalysis for Sustainable Energy: Hydrogen and Methanol Economies, Fuels from Biomass, and Related Topics. Chem. Rev. 122, 385–441. https://doi.org/10.1021/acs.chemrev.1c00412.

9. Arsad, A.Z., Hannan, M.A., Al-Shetwi, A.Q., Mansur, M., Muttaqi, K.M., Dong, Z.Y., and Blaabjerg, F. (2022). Hydrogen energy storage integrated hybrid renewable energy systems: A review analysis for future research directions. Int. J. Hydrogen Energy 47, 17285–17312. https://doi.org/10.1016/j.ijhydene.2022.03.208.

10. Farias, C.B.B., Barreiros, R.C.S., da Silva, M.F., Casazza, A.A., Converti, A., and Sarubbo, L.A. (2022). Use of Hydrogen as Fuel: A Trend of the 21st Century. Energies 15, 311.

11. Xiao, X., Yang, L., Sun, W., Chen, Y., Yu, H., Li, K., Jia, B., Zhang, L., and Ma, T. (2022). Electrocatalytic Water Splitting: From Harsh and Mild Conditions to Natural Seawater. Small 18, 2105830. https://doi.org/10.1002/smll.202105830.

12. Carmel, L., Aharon, S., Meyerstein, D., Albo, Y., Friedlander, L., Shamir, D., and Burg, A. (2024). WO3 dehydration and phase transition as the catalytic driver of hydrogen production by non-calcinated WO3. Int. J. Hydrogen Energy 51, 1508–1520. https://doi.org/10.1016/j.ijhydene.2023.07.351.

13. Qu, H.-Y., He, X., Wang, Y., and Hou, S. (2021). Electrocatalysis for the Oxygen Evolution Reaction in Acidic Media: Progress and Challenges. Appl. Sci. 11, 4320.

14. Saha, E., Karthick, K., Kundu, S., and Mitra, J. (2019). Electrocatalytic Oxygen Evolution in Acidic and Alkaline Media by a Multistimuli-Responsive Cobalt(II) Organogel. ACS Sustain. Chem. Eng. 7, 16094–16102. https://doi.org/10.1021/acssuschemeng.9b02858.

15. Wang, D., and Bruner, C.O. (2017). Catalytic Water Oxidation by a Bio-inspired Nickel Complex with a Redox-Active Ligand. Inorg. Chem. 56, 13638–13641. https://doi.org/10.1021/acs.inorgchem.7b02166.

16. Wang, T., He, H., Meng, Z., Li, S., Xu, M., Liu, X., Zhang, Y., Liu, M., and Feng, M. (2023). Magnetic Field-Enhanced Electrocatalytic Oxygen Evolution on a Mixed-Valent Cobalt-Modulated LaCoO3 Catalyst. ChemPhysChem 24, e202200845. https://doi.org/10.1002/cphc.202200845.

17. Kumar, M., Piccinin, S., and Srinivasan, V. (2022). Direct and indirect role of Fe doping in NiOOH monolayer for water oxidation catalysis. ChemPhysChem 23, e202200085. https://doi.org/10.1002/cphc.202200085.

18. Zeng, F., Mebrahtu, C., Liao, L., Beine, A.K., and Palkovits, R. (2022). Stability and deactivation of OER electrocatalysts: A review. J. Energy Chem. 69, 301–329. https://doi.org/10.1016/j.jechem.2022.01.025.

19. Xue, H., Meng, A., Yang, T., Li, Z., and Chen, C. (2022). Controllable oxygen vacancies and morphology engineering: Ultra-high HER/OER activity under base–acid conditions and outstanding antibacterial properties. J. Energy Chem. 71, 639–651. https://doi.org/10.1016/j.jechem.2022.04.052.

20. Liang, Q., Brocks, G., and Bieberle-Hütter, A. (2021). Oxygen evolution reaction (OER) mechanism under alkaline and acidic conditions. J. Phys.: Energy 3, 026001. https://doi.org/10.1088/2515-7655/abdc85.

21. Hu, Q., Li, G., Liu, X., Zhu, B., Li, G., Fan, L., Chai, X., Zhang, Q., Liu, J., and He, C. (2019). Coupling pentlandite nanoparticles and dual-doped carbon networks to yield efficient and stable electrocatalysts for acid water oxidation. J. Mater. Chem. A 7, 461–468. https://doi.org/10.1039/C8TA09534E.

22. Huynh, M., Ozel, T., Liu, C., Lau, E.C., and Nocera, D.G. (2017). Design of template-stabilized active and earth-abundant oxygen evolution catalysts in acid. Chem. Sci. 8, 4779–4794. https://doi.org/10.1039/C7SC01239J.

23. Kim, H.J., Kim, H.Y., Joo, J., Joo, S.H., Lim, J.S., Lee, J., Huang, H., Shao, M., Hu, J., Kim, J.Y., et al. (2022). Recent advances in non-precious group metal-based catalysts for water electrolysis and beyond. J. Mater. Chem. A 10, 50–88. https://doi.org/10.1039/D1TA06548C.

24. Liu, P.F., Yin, H., Fu, H.Q., Zu, M.Y., Yang, H.G., and Zhao, H. (2020). Activation strategies of water-splitting electrocatalysts. J. Mater. Chem. A 8, 10096–10129. https://doi.org/10.1039/D0TA01680B.

25. Siddiqi, G., Luo, Z., Xie, Y., Pan, Z., Zhu, Q., Röhr, J.A., Cha, J.J., and Hu, S. (2018). Stable Water Oxidation in Acid Using Manganese-Modified TiO2 Protective Coatings. ACS Appl. Mater. Interfaces 10, 18805–18815. https://doi.org/10.1021/acsami.8b05323.

26. Thorarinsdottir, A.E., and Nocera, D.G. (2021). Energy catalysis needs ligands with high oxidative stability. Chem Catal. 1, 32–43. https://doi.org/10.1016/j.checat.2021.05.012.

27. Aharon, S., Patra, S.G., Meyerstein, D., Tzur, E., Shamir, D., Albo, Y., and Burg, A. (2023). Heterogeneous Electrocatalytic Oxygen Evolution Reaction by a Sol-Gel Electrode with Entrapped Na3[Ru2(μ-CO3)4]: The Effect of NaHCO3. ChemPhysChem 24, e202300517. https://doi.org/10.1002/cphc.202300517.

28. Spöri, C., Kwan, J.T.H., Bonakdarpour, A., Wilkinson, D.P., and Strasser, P. (2017). The Stability Challenges of Oxygen Evolving Catalysts: Towards a Common Fundamental Understanding and Mitigation of Catalyst Degradation. Angew. Chem. Int. Ed. 56, 5994–6021. https://doi.org/10.1002/anie.201608601.

29. Koper, M.T.M. (2011). Thermodynamic theory of multi-electron transfer reactions: Implications for electrocatalysis. J. Electroanal. Chem. 660, 254–260. https://doi.org/10.1016/j.jelechem.2010.10.004.

30. Fan, M., Liang, X., Chen, H., and Zou, X. (2020). Low-iridium electrocatalysts for acidic oxygen evolution. Dalton Trans. 49, 15568–15573. https://doi.org/10.1039/D0DT02676J.

31. Hu, W., Zhong, H., Liang, W., and Chen, S. (2014). Ir-Surface Enriched Porous Ir–Co Oxide Hierarchical Architecture for High Performance Water Oxidation in Acidic Media. ACS Appl. Mater. Interfaces 6, 12729–12736. https://doi.org/10.1021/am5027192.

32. Cui, X. (2022). Introducing hydrogen bonds in RuO2 boosts acidic OER activity and stability. Chem Catal. 2, 431–433. https://doi.org/10.1016/j.checat.2022.02.011.

33. Mondschein, J.S., Callejas, J.F., Read, C.G., Chen, J.Y.C., Holder, C.F., Badding, C.K., and Schaak, R.E. (2017). Crystalline Cobalt Oxide Films for Sustained Electrocatalytic Oxygen Evolution under Strongly Acidic Conditions. Chem. Mater. 29, 950–957. https://doi.org/10.1021/acs.chemmater.6b02879.

34. Gumerova, N.I., and Rompel, A. (2020). Polyoxometalates in solution: speciation under spotlight. Chem. Soc. Rev. 49, 7568–7601. https://doi.org/10.1039/D0CS00392A.

35. Gao, D., Trentin, I., Schwiedrzik, L., González, L., and Streb, C. (2020). The Reactivity and Stability of Polyoxometalate Water Oxidation Electrocatalysts. Molecules 25, 157.

36. Mukhopadhyay, S., Debgupta, J., Singh, C., Kar, A., and Das, S.K. (2018). A Keggin Polyoxometalate Shows Water Oxidation Activity at Neutral pH: POM@ZIF-8, an Efficient and Robust Electrocatalyst. Angew. Chem. Int. Ed. 57, 1918–1923. https://doi.org/10.1002/anie.201711920.

37. Mulkapuri, S., Ravi, A., Nasani, R., Kurapati, S.K., and Das, S.K. (2022). Barrel-Shaped-Polyoxometalates Exhibiting Electrocatalytic Water Reduction at Neutral pH: A Synergy Effect. Inorg. Chem. 61, 13868–13882. https://doi.org/10.1021/acs.inorgchem.2c01811.

38. Vazylyev, M., Sloboda-Rozner, D., Haimov, A., Maayan, G., and Neumann, R. (2005). Strategies for oxidation catalyzed by polyoxometalates at the interface of homogeneous and heterogeneous catalysis.

39. Top. Catal. 34, 93–99. https://doi.org/10.1007/s11244-005-3793-5.

39. Zahran, Z.N., Tsubonouchi, Y., Mohamed, E.A., and Yagi, M. (2019). Recent Advances in the Development of Molecular Catalyst-Based Anodes for Water Oxidation toward Artificial Photosynthesis. ChemSusChem 12, 1775–1793. https://doi.org/10.1002/cssc.201802795.

40. Blasco-Ahicart, M., Soriano-López, J., Carbó, J.J., Poblet, J.M., and Galan-Mascaros, J.R. (2018). Polyoxometalate electrocatalysts based on earth-abundant metals for efficient water oxidation in acidic media. Nat. Chem. 10, 24–30. https://doi.org/10.1038/nchem.2874.

41. Gao, Y., Choudhari, M., Such, G.K., and Ritchie, C. (2022). Polyoxometalates as chemically and structurally versatile components in self-assembled materials. Chem. Sci. 13, 2510–2527. https://doi.org/10.1039/D1SC05879G.

42. Wang, S., Wang, X., Sun, C., and Wu, Z.-S. (2021). Room-temperature fast assembly of 3D macroscopically porous graphene frameworks for binder-free compact supercapacitors with high gravimetric and volumetric capacitances. J. Energy Chem. 61, 23–28. https://doi.org/10.1016/j.jechem.2021.01.019.

43. Fu, W., Han, C., Li, D., Chen, W., Ji, J., Qian, G., Yuan, W., Duan, X., and Zhou, X. (2020). Polyoxometalates-engineered hydrogen generation rate and durability of Pt/CNT catalysts from ammonia borane. J. Energy Chem. 41, 142–148. https://doi.org/10.1016/j.jechem.2019.05.014.

44. Wu, Z., Li, Y., Zhang, C., Huang, X., Peng, B., and Wang, G. (2022). Recent advances in metal-organic-framework-based catalysts for thermocatalytic selective oxidation of organic substances. Chem Catal. 2, 1009–1045. https://doi.org/10.1016/j.checat.2022.02.010.

45. Liu, Q., and Wang, X. (2022). Sub-nanometric materials: Electron transfer, delocalization, and beyond. Chem Catal. 2, 1257–1266. https://doi.org/10.1016/j.checat.2022.03.008.

46. Coronel, N.C., and da Silva, M.J. (2018). Lacunar Keggin Heteropolyacid Salts: Soluble, Solid and Solid-Supported Catalysts. J. Cluster Sci. 29, 195–205. https://doi.org/10.1007/s10876-018-1343-0.

47. Li, S.-W., Zhang, H.-Y., Dong, S.-M., Zhao, J.-S., and Li, R.-X. (2022). Highly efficient preformed heteropolyacid catalysts for the deep oxidative desulfurization: MOF as a bridge role under nucleation theory. J. Environ. Chem. Eng. 10, 107298. https://doi.org/10.1016/j.jece.2022.107298.

48. Sullivan, K.P., Yin, Q., Collins-Wildman, D.L., Tao, M., Geletii, Y.V., Musaev, D.G., Lian, T., and Hill, C.L. (2018). Multi-Tasking POM Systems. Front. Chem. 6, 365. https://doi.org/10.3389/fchem.2018.00365.

49. Azmani, K., Besora, M., Soriano-López, J., Landolsi, M., Teillout, A.-L., de Oliveira, P., Mbomekallé, I.-M., Poblet, J.M., and Galán-Mascarós, J.-R. (2021). Understanding polyoxometalates as water oxidation catalysts through iron vs. cobalt reactivity. Chem. Sci. 12, 8755–8766. https://doi.org/10.1039/D1SC01016F.

50. Bakuru, V.R., DMello, M.E., and Kalidindi, S.B. (2019). Metal-Organic Frameworks for Hydrogen Energy Applications: Advances and Challenges. ChemPhysChem 20, 1177–1215. https://doi.org/10.1002/cphc.201801147.

51. Shahsavarifar, S., Masteri-Farahani, M., and Ganjali, M.R. (2022). Design and application of a polyoxometalate-ionic liquid-graphene oxide hybrid nanomaterial: New electrocatalyst for water oxidation. Colloids Surf. A Physicochem. Eng. Asp. 632, 127812. https://doi.org/10.1016/j.colsurfa.2021.127812.

52. Sartorel, A., Carraro, M., Scorrano, G., Zorzi, R.D., Geremia, S., McDaniel, N.D., Bernhard, S., and Bonchio, M. (2008). Polyoxometalate Embedding of a Tetraruthenium(IV)-oxo-core by Template-Directed Metalation of [γ-SiW10O36]8−: A Totally Inorganic Oxygen-Evolving Catalyst. J. Am. Chem. Soc. 130, 5006–5007. https://doi.org/10.1021/ja077837f.

53. Huang, Z., Luo, Z., Geletii, Y.V., Vickers, J.W., Yin, Q., Wu, D., Hou, Y., Ding, Y., Song, J., Musaev, D.G., et al. (2011). Efficient Light-Driven Carbon-Free Cobalt-Based Molecular Catalyst for Water Oxidation. J. Am. Chem. Soc. 133, 2068–2071. https://doi.org/10.1021/ja109681d.

54. Gerken, J.B., McAlpin, J.G., Chen, J.Y.C., Rigsby, M.L., Casey, W.H., Britt, R.D., and Stahl, S.S. (2011). Electrochemical Water Oxidation with Cobalt-Based Electrocatalysts from pH 0–14: The Thermodynamic Basis for Catalyst Structure, Stability, and Activity. J. Am. Chem. Soc. 133, 14431–14442. https://doi.org/10.1021/ja205647m.

55. Haider, A., Bassil, B.S., Soriano-López, J., Qasim, H.M., Sáenz de Pipaón, C., Ibrahim, M., Dutta, D., Koo, Y.-S., Carbó, J.J., Poblet, J.M., et al. (2019). 9-Cobalt(II)-Containing 27-Tungsto-3-germanate(IV): Synthesis, Structure, Computational Modeling, and Heterogeneous Water Oxidation Catalysis. Inorg. Chem. 58, 11308–11316. https://doi.org/10.1021/acs.inorgchem.9b01495.

56. Yin, Q., Tan, J.M., Besson, C., Geletii, Y.V., Musaev, D.G., Kuznetsov, A.E., Luo, Z., Hardcastle, K.I., and Hill, C.L. (2010). A Fast Soluble Carbon-Free Molecular Water Oxidation Catalyst Based on Abundant Metals. Science 328, 342–345. https://doi.org/10.1126/science.1185372.

57. Xin, Y., Ma, L., Bai, Y., Zhao, Y., and Li, G. (2022). Effective heterogeneous catalysis of micro-size H3PMo6W6O40@rht-MOF-1 for degradation of phenolic compounds under molecular oxygen. J. Environ. Chem. Eng. 10, 108772. https://doi.org/10.1016/j.jece.2022.108772.

58. Mialane, P., Mellot-Draznieks, C., Gairola, P., Duguet, M., Benseghir, Y., Oms, O., and Dolbecq, A. (2021). Heterogenisation of polyoxometalates and other metal-based complexes in metal–organic frameworks: from synthesis to characterisation and applications in catalysis. Chem. Soc. Rev. 50, 6152–6220. https://doi.org/10.1039/D0CS00323A.

59. Silva, D.F., Viana, A.M., Santos-Vieira, I., Balula, S.S., and Cunha-Silva, L. (2022). Ionic Liquid-Based Polyoxometalate Incorporated at ZIF-8: A Sustainable Catalyst to Combine Desulfurization and Denitrogenation Processes. Molecules 27, 1711.

60. Singh, C., Mukhopadhyay, S., and Das, S.K. (2018). Polyoxometalate-Supported Bis(2,2′-bipyridine)mono(aqua)nickel(II) Coordination Complex: an Efficient Electrocatalyst for Water Oxidation. Inorg. Chem. 57, 6479–6490. https://doi.org/10.1021/acs.inorgchem.8b00541.

61. Burg, A., Shamir, D., Apelbaum, L., Albo, Y., Maimon, E., and Meyerstein, D. (2016).

Electrocatalytic Oxidation of Amines by Ni–(1,4,8,11-tetraazacyclotetradecane)2+ Entrapped in Sol–Gel Electrodes. Eur. J. Inorg. Chem. *2016*, 459–463. https://doi.org/10.1002/ejic.201690006.

62. Shamir, D., Elias, I., Albo, Y., Meyerstein, D., and Burg, A. (2020). ORMOSIL-entrapped copper complex as electrocatalyst for the heterogeneous de-chlorination of alkyl halides. Inorg. Chim. Acta. *500*, 119225. https://doi.org/10.1016/j.ica.2019.119225.

63. Rabinovich, L., and Lev, O. (2001). Sol-Gel Derived Composite Ceramic Carbon Electrodes. Electroanalysis *13*, 265–275. https://doi.org/10.1002/1521-4109(200103)13:4<265::AID-ELAN265>3.0.CO.

64. Aharon, S., Meyerstein, D., Tzur, E., Shamir, D., Albo, Y., and Burg, A. (2021). Advanced sol–gel process for efficient heterogeneous ring-closing metathesis. Sci. Rep. *11*, 12506. https://doi.org/10.1038/s41598-021-92043-z.

65. Peled, Y., Shamir, D., Marks, V., Kornweitz, H., Albo, Y., Yakhin, E., Meyerstein, D., and Burg, A. (2022). Sol-gel matrices for the separation of uranyl and other heavy metals. J. Environ. Chem. Eng. *10*, 108142. https://doi.org/10.1016/j.jece.2022.108142.

66. Biton Seror, S., Shamir, D., Albo, Y., Kornweitz, H., and Burg, A. (2022). Elucidation of a mechanism for the heterogeneous electro-fenton process and its application in the green treatment of azo dyes. Chemosphere *286*, 131832. https://doi.org/10.1016/j.chemosphere.2021.131832.

67. Neelam, Meyerstein, D., Burg, A., Shamir, D., and Albo, Y. (2018). Polyoxometalates entrapped in sol-gel matrices as electron exchange columns and catalysts for the reductive de-halogenation of halo-organic acids in water. J. Coord. Chem. *71*, 3180–3193. https://doi.org/10.1080/00958972.2018.1515926.

68. Neelam, Albo, Y., Shamir, D., Burg, A., Palaniappan, S., Goobes, G., and Meyerstein, D. (2016). Polyoxometalates entrapped in sol–gel matrices for reducing electron exchange column applications. J. Coord. Chem. *69*, 3449–3457. https://doi.org/10.1080/00958972.2016.1245418.

69. Song, Y., Peng, Y., Yao, S., Zhang, P., Wang, Y., Gu, J., Lu, T., and Zhang, Z. (2022). Co-POM@MOF-derivatives with trace cobalt content for highly efficient oxygen reduction. Chin. Chem. Lett. *33*, 1047–1050. https://doi.org/10.1016/j.cclet.2021.08.045.

70. Gao, G.-G., Xu, L., Wang, W.-J., Qu, X.-S., Liu, H., and Yang, Y.-Y. (2008). Cobalt(II)/Nickel(II)-Centered Keggin-Type Heteropolymolybdates: Syntheses, Crystal Structures, Magnetic and Electrochemical Properties. Inorg. Chem. *47*, 2325–2333. https://doi.org/10.1021/ic700797v.

71. Wang, C.-J., Yao, S., Chen, Y.-Z., Zhang, Z.-M., and Wang, E.-B. (2016). Assembly of polyoxometalates and Ni-bpy cationic units into the molecular core–shell structures as bifunctional electrocatalysts. RSC Adv. *6*, 99010–99015. https://doi.org/10.1039/C6RA19257B.

72. Shahadat, H.M., Younus, H.A., Ahmad, N., Rahaman, M.A., Khattak, Z.A.K., Zhuiykov, S., and Verpoort, F. (2019). Homogenous electrochemical water oxidation by a nickel(ii) complex based on a macrocyclic N-heterocyclic carbene/pyridine hybrid ligand. Catal. Sci. Technol. *9*, 5651–5659. https://doi.org/10.1039/C9CY01485C.

73. Krishna, J.V.S., Krishna, N.V., Singh, S.K., Shaw, P.K., Dhavale, V.M., Vardhaman, A.K., and Giribabu, L. (2018). Substituent-Induced Deformed Ni–Porphyrin as an Electrocatalyst for the Electrochemical Conversion of Water into Dioxygen. Eur. J. Inorg. Chem. *2018*, 1549–1555. https://doi.org/10.1002/ejic.201701427.

74. McCrory, C.C.L., Jung, S., Peters, J.C., and Jaramillo, T.F. (2013). Benchmarking Heterogeneous Electrocatalysts for the Oxygen Evolution Reaction. J. Am. Chem. Soc. *135*, 16977–16987. https://doi.org/10.1021/ja407115p.

75. Patra, S.G., Mizrahi, A., and Meyerstein, D. (2020). The Role of Carbonate in Catalytic Oxidations. Acc. Chem. Res. *53*, 2189–2200. https://doi.org/10.1021/acs.accounts.0c00344.

76. Lei, J., Yang, J.-J., Liu, T., Yuan, R.-M., Deng, D.-R., Zheng, M.-S., Chen, J.-J., Cronin, L., and Dong, Q.-F. (2019). Tuning Redox Active Polyoxometalates for Efficient Electron-Coupled Proton-Buffer-Mediated Water Splitting. Chem. Eur. J *25*, 11432–11436. https://doi.org/10.1002/chem.201903142.

77. Schubert, U. (2015). Chemistry and Fundamentals of the Sol–Gel Process. In The Sol-Gel Handbook, pp. 1–28. https://doi.org/10.1002/9783527670819.ch01.

78. Schubert, U. (2015). Chemistry and Fundamentals of the Sol–Gel Process. In The Sol-Gel Handbook, pp. 1–28. https://doi.org/10.1002/9783527670819.ch01.

79. Vickers, J.W., Lv, H., Sumliner, J.M., Zhu, G., Luo, Z., Musaev, D.G., Geletii, Y.V., and Hill, C.L. (2013). Differentiating Homogeneous and Heterogeneous Water Oxidation Catalysis: Confirmation that [Co4(H2O)2(α-PW9O34)2]10– Is a Molecular Water Oxidation Catalyst. J. Am. Chem. Soc. *135*, 14110–14118. https://doi.org/10.1021/ja4024868.

80. Baker, L.C.W., and McCutcheon, T.P. (1956). Heteropoly Salts Containing Cobalt and Hexavalent Tungsten in the Anion1. J. Am. Chem. Soc. *78*, 4503–4510. https://doi.org/10.1021/ja01599a001.

81. Pintado, S., Goberna-Ferrón, S., Escudero-Adán, E.C., and Galán-Mascarós, J.R. (2013). Fast and Persistent Electrocatalytic Water Oxidation by Co–Fe Prussian Blue Coordination Polymers. J. Am. Chem. Soc. *135*, 13270–13273. https://doi.org/10.1021/ja406242y.

STAR★METHODS

KEY RESOURCES TABLE

REAGENT or RESOURCE	SOURCE	IDENTIFIER
Chemicals, peptides, and recombinant proteins		
Cobalt acetate	Sigma-Aldrich	CAS# 71-48-7
Glacial acetic acid	Sigma-Aldrich	CAS# 64-19-7
Graphite	Sigma-Aldrich	CAS# 7782-42-5
Hydrochloric acid	Sigma-Aldrich	CAS# 7647-01-0
Potassium chloride	Sigma-Aldrich	CAS# 7447-40-7
Tetramethyl orthosilicates (TMOS)	Sigma-Aldrich	CAS# 681-84-5
Sodium perchlorate	Sigma-Aldrich	CAS# 7601-89-0
Sodium tungstate dihydrate	Sigma-Aldrich	CAS# 10213-10-2
Ultrapure water with a final resistance of 18.2 MΩ cm	TKA-GenPure	Cat# 50131217
Software and algorithms		
PSTrace 5.9 software	PalmSens BV	https://www.palmsens.com/software/ps-trace/
Origin 8.5 software	OriginLab Corporation	https://www.originlab.com/
Other		
X-ray Powder Diffraction (PXRD)	PanAnalytical	Empyrean III
Fourier transform infrared spectroscopy	Nicolet	Impact 410
Raman spectral analysis	Horiba	LabRam HR Evolution
X-ray photoelectron spectroscopy (XPS)	Thermo Fisher	ESCALAB™ QXi X-ray Photoelectron Spectrometer Microprobe
Scanning Electron Microscopy (SEM)	TESCAN	VEGA4LMS
Cryogenic Scanning Electron Microscopy (Cryo-SEM)	ZEISS	Gemini 300
Elemental analysis by Inductively Coupled Plasma Optical Emission Spectroscopy (ICP-OES)	SPECTRO	ARCOS

RESOURCE AVAILABILITY

Lead contact

Further information and requests for resources should be directed to and will be fulfilled by the lead contact, Ariela Burg (arielab@sce.ac.il).

Materials availability

This study did not generate new materials.

Data and code availability

- This paper does not report original code.
- Any additional information required to reanalyze the data reported in this paper is available from the lead contact upon request.

METHOD DETAILS

The research was composed from four main stages: 1. Co-POM synthesis, 2. Electrodes preparation according to a published procedure. 3. Characterization of the Co-POM and the electrodes by various methods. 4. Electrochemistry experiments.

Materials

All chemical reagents were of analytical grade and used without further purification. All solutions were freshly prepared with ultrapure water.

Co-POM synthesis

$K_6[CoW_{12}O_{40}]$ (Co-POM): The Keggin POM, $K_6[CoW_{12}O_{40}]$, was synthesized by slightly modifying the reported procedure in the literature.[60,80] The synthetic process is as follows:

A solution of sodium tungstate dehydrate was prepared, and the pH of the solution was adjusted to 6.5–7.5 by the addition of glacial acetic acid. This solution was heated to near boiling point and to this a solution of cobalt acetate was added dropwise while stirring. The mixture was boiled for 10 min and then filtered in hot conditions. Then a hot aqueous saturated KCl solution was added to the filtrate, and the mixture was kept for 24 h in room temperature. The green precipitate formed was separated, and 2M sulfuric acid was added to it. Then the mixture was boiled to decrease the volume and filtered. The filtrate was kept in an ice bath for 24 h to obtain good-quality bluish-green crystals, which were separated using Buckner funnel, washed with ice-cold water, and then dried in air.

Co-POM was characterized by powder-XRD (PXRD) and FT-IR (Figures S2 and S3) before incorporating into the sol-gel electrodes.

Working electrode preparation

Working Electrode preparation (Co-POM-TMOS): The sol-gel electrodes were prepared by optimizing the literature protocol according to our needs.[61–63,66] The starting mixture of Co-POM-TMOS sol-gel electrode comprises TMOS (300 μL, 2 mmol), Graphite (0.15 g, 12.5 mmol), and aqueous solution of Co-POM (1 mmol of Co-POM in 600 μL (33.3 mmol) H_2O). The pH of the aqueous solution of the Co-POM was adjusted to 2.0 by adding 0.1 M HCl before adding it to the mixture for electrode preparation. The slurry obtained was mixed until a single phase was acquired, then transferred to a homemade electrode holder and kept for air drying for 3 weeks for porous heterogeneous electrode fabrication (Figure S1).

Blank electrode preparation

Blank electrode preparation (TMOS): The TMOS sol-gel electrode preparation methodology is similar to Co-POM-TMOS electrode preparation, with the only difference of having no Co-POM in its mixture.

Characterization methods

Sample characterization was performed by X-ray Powder Diffraction (PXRD) on an Empyrean III (panalytical). X-ray diffractometer with the X-ray source: Philips ceramic sealed tube (1.8kW) with the wavelength: Cu Kα (1.5405 Å).

Infrared (FTIR) spectra were acquired from KBr pellets using a Nicolet Impact 410 spectrophotometer.

Raman spectral analysis was performed on LabRam HR Evolution Horiba Raman with laser of 532 nm.

X-ray photoelectron spectroscopy (XPS) studies were performed on ESCALAB QXi X-ray Photoelectron Spectrometer Microprobe.

Scanning Electron Microscope (SEM) images and Energy-dispersive X-ray spectra (EDS/EDX) were acquired using Desktop Scanning Electron Microscope (Tescan VEGA4LMS + Oxford 15mm EDS AztekOne) and Cryogenic Scanning Electron Microscopy (Gemini 300, ZEISS cryo-SEM, and LEICA sample preparation equipment.

Elemental analysis of ions in solutions after electrochemical studies was performed by Inductively Coupled Plasma Optical Emission Spectroscopy (ICP-OES) using an SPECTRO model ARCOS.

Electrochemical studies

All the electrochemical experiments were carried out using a PalmSens EmStat3 potentiostat operated with PSTrace 5.9 software. Electrochemical experiments were accomplished using a three-electrode electrochemical cell using prepared sol-gel electrodes as working electrodes, Ag/AgCl (3 M) as reference electrodes and Pt-Wire as counter electrodes. Using 0.20 M $NaClO_4$, pH 2.0 as an electrolyte. For the connection of the sol-gel electrodes to the cell, dry graphite powder of around 200 mg is added on top of the dried electrodes, (Figure S1) and a platinum wire was inserted through the dry Graphite to complete the circuit without damaging the electrodes. The surface area of the outer exposed part of the sol-gel electrodes is 0.077 cm^2 and is used to calculate current density. Cyclic voltammetry scans were recorded by scanning the anodic side first, followed by a cathodic scan. Three cycles were taken consecutively for each set of cyclic voltammetry measurements. Cyclic voltammograms (CVs) were also recorded at various scan rates. Linear Sweep Voltammograms (LSVs) were initiated at the open circuit potential (OCP). The represented cyclic voltammogram (CV) in the article is the 2nd cycle of CV scan. Glassy carbon, with a geometrical area of 0.071 cm^2, was used to record homogeneous electrochemical measurements. All the electrochemical measurements are converted into NHE by using Equation 12:

$$E(NHE) = E(Ag/AgCl) + 0.197 \qquad \text{(Equation 12)}$$

The electrochemical impedance spectroscopy (EIS) measurements were recorded using a PalmSens EmStat4s potentiostat, and the Nyquist plots were fitted with PalmSens software PSTrace 5.9.

QUANTIFICATION AND STATISTICAL ANALYSIS

PSTrace 5.9 software was used to operate the potentiostat, collect electrochemical data and fit the Nyquist plots. Origin 8.5 software was used to compile figures and analyze data.

Calculation of surface coverage and number of active cobalt atoms

We have calculated the active Co atoms/cm^2 on the electrode surface using a method described in the literature[81] by measuring the surface coverage (Γ_0) from the slope (2.02×10^{-4} F) of the i_p vs. scan rate (Figure S9) using the Equation 13.

$$Slope = n^2F^2A\Gamma_0/4RT \qquad \text{(Equation 13)}$$

Where 'n' = No. of electrons involved, here 1, For Co(II) – Co(III) conversion.

'F' = 1 F = 96,500 C.

'A' = Geometrical surface area of electrode.

'R' = Ideal Gas Constant.

'T' = Temperature during experiment (298 K).

'Γ_0' = Surface density of active cobalt atoms.

Thus, obtained surface density of active cobalt atoms is **2.95×10^{-9} mol/cm^2**.

Calculation of turnover frequencey (TOF) for O$_2$ evolution from Tafel plot

The activity of a catalyst can be well-expressed in terms of turn over frequency (TOF). It is defined as the number of reactant molecules getting converted into product molecules in unit time per active site. The TOF is measured as follows in Equation 14:

$$TOF\ at\ any\ given\ over\ potential\ = \frac{Current\ density\ at\ given\ over\ potential}{4 \times F \times No.\ of\ active\ cobalt} \qquad \text{(Equation 14)}$$

Here, 4 appears because OER is a 4e-process. Hence division of current density at a particular overpotential by 4F (F = Faraday constant) gives one catalytic turnover number and further division of turnover number by the number of active cobalt atoms results in turnover frequency (TOF).

$$TOF_{j\ =\ 2\ mA/cm^2}\ = \frac{2 * 10^{-3}}{4 \times F \times 2.95 * 10^{-9}} \qquad \text{(Equation 15)}$$

Thus (TOF) $_{j=2\ mA}$ = **1.76 [mol O$_2$ (mol Co)$^{-1}$s^{-1}]**.